Identifiability of stiffness components of clear wood from a single off-axes compression test

J. Xavier[a], A. Majano-Majano[b], Jose Fernandez-Cabo[b]

[a] *CITAB, UTAD, Engenharias I, Apartado 1013, 5001-801 Vila Real, Portugal*
[b] *ETS of Architecture, Structural Department, Technical University of Madrid (UPM), Madrid, Spain*

Abstract

In this work, the identifiability of orthotropic stiffness components of clear wood from a single off-axis compression test was investigated. The parameter identification strategy was based on anisotropic elasticity theory, so-called anisotropic-based method. The proposed approach couples off-axes compression tests on prismatic specimens with 3D full-field measurements. In practice, these measurements can be provided by a suitable optical technique such as stereovision or ESPI. Experimentally, specific tests were carried out in order to deal with boundary issues such as friction and shear-extension coupling effects. Numerically, a finite element model of the mechanical test was built as a support for optimal inspection the test configuration in terms of angles orientation (direction cosine matrix), such that balanced strain components can be reached in the material coordinate system. Results, conclusions and future work were discussed in view of the identifiability of all active stiffness components from only one test configuration.

Keywords: Wood, Digital image correlation, material parameter identification, Compression tests

1. Introduction

The parameters governing constitutive equations of materials are determined experimentally by means of suitable mechanical tests. In the field of solid mechanics, this issue is presented as an inverse problem where the material parameters are to be determined from the knowledge of geometry, boundary conditions and strains (or displacements). Conventionally, this identification is achieved by carrying out mechanical tests in which specimen geometry and loading system are designed to generate homogeneous or simple strain/stress states across the gauge region. The underlying idea behind this assumption is useful for theoretical analyses because closed-form solutions can be obtained, relating the unknown material parameters to the load and strain measurements (statically determined tests).

However, the practical implementation of these tests can be difficult, especially for anisotropic and heterogeneous materials such as wood. The recent development of full-field optical techniques has enabled a new glance on the mechanical tests for material characterisation. The basic idea driving this new approach is that a single specimen can be loaded in order that several parameters are involved in the mechanical response, yielding heterogeneous and complex strain fields (statically undetermined tests). By means of a suitable identification strategy all the active parameters can be determined afterwards.

Wood is a biological composite material formed by trees. It can be analysed at several scales of observation from timber down to chemical constituents. The mechanisms of deformation in wood can be quite complex involving, for instance, anisotropic, viscoelastic and hygroscopic phenomena. Moreover, the intra and inter variability of wood is reflected on the material parameters governing relevant constitutive equations. Therefore, the investigation of the wood mechanical behaviour raises several difficulties from both modelling and experimental points of view. In most practical applications and with some simplification hypothesis, invoking low levels of stress, short periods of time and minor variations of moisture content and temperature, wood can be modelled as a linear elastic anisotropic material. Besides, at the macro scale (0.1-1 m) wood is usually assumed as a continuum and homogeneous medium. The complete characterisation of the linear elastic orthotropic behaviour of clear wood requires the determination of nine independent stiffness components. Conventionally, this set of material parameters are determined experimentally by carrying out several test methods, in which both loading and specimen geometry are usually oriented along the material directions. Moreover, these tests are based on the assumption of simple and homogeneous stress/strain states across the elementary representative volume of the material at the scale of observation. This approach represents a great effort from an experimental point of view because only a few (*i.e.*, one or two) stiffness components are obtained per test configuration. Besides, the complete stiffness matrix will be characterised from different test and specimen configurations, enhancing variability. In order to overcome these limitations, a single off-axes compression test method for clear wood has been recently proposed [1]. This project aims further improvements of the test method with regard to the identifiability of the whole set of orthotropic stiffness components. Both experimental and numerical analysis will be addressed. 3D full-field measurements provided by a stereovision and EPSI will be envisaged. Preliminary tests were carried out in order to deal with boundary issues such as friction and shear-extension coupling effects, coupling off-axes compression tests with stereosivion technique (ARAMIS® system by GOM). Numerically, finite element analyses of the mechanical test method were performed in order to optimise the test configuration in terms of angles orientation (direction

cosine matrix), such that balanced strain components are reached in the material coordinate system.

2. Identification strategy: Anisotropic-based method

Let us consider the compression test schematically represented in Fig. 1. In this mechanical model, a rectangular prismatic specimen with nominal dimensions L (length)$\times$ w (width) $\times$ t (thickness) is submitted to a uniform and uniaxial compression stress state at its ends. It is assumed that the material is continuous, homogeneous and governed by a linear elastic orthotropic behaviour. The identification strategy used in this work was based on anisotropic elasticity theory. The focus was given to the identification of the orthotropic linear elastic behaviour of wood at the macroscopic scale. In the specific case where material and specimen coordinate systems are coincident, S_{123} (with $123 \equiv LRT$), the generalised Hooke's law writes as (in Voigt notation)

$$\begin{Bmatrix} \varepsilon_{11} \\ \varepsilon_{22} \\ \varepsilon_{33} \\ \gamma_{23} \\ \gamma_{13} \\ \gamma_{12} \end{Bmatrix} = \begin{bmatrix} S_{11} & S_{12} & S_{13} & 0 & 0 & 0 \\ S_{12} & S_{22} & S_{23} & 0 & 0 & 0 \\ S_{13} & S_{23} & S_{33} & 0 & 0 & 0 \\ 0 & 0 & 0 & S_{44} & 0 & 0 \\ 0 & 0 & 0 & 0 & S_{55} & 0 \\ 0 & 0 & 0 & 0 & 0 & S_{66} \end{bmatrix} \begin{Bmatrix} \sigma_{11} \\ \sigma_{22} \\ \sigma_{33} \\ \tau_{23} \\ \tau_{13} \\ \tau_{12} \end{Bmatrix} \quad \Rightarrow \quad \{\varepsilon\} = [S]\{\sigma\} \qquad (1)$$

where $\{\varepsilon\}$ is the engineering strain pseudo-vector ([6×1]), $\{\sigma\}$ is the Cauchy stress pseudo-vector ([6×1]), and $[S]$ is the compliance matrix ([6×6]). The elements of $[S]$ can be written as function of the 9 independent engineering elastic constants: E_L, E_R, E_T, ν_{RT}, ν_{LT}, ν_{LR}, G_{RT}, G_{LT} and G_{LR} where E, ν and G stands for Young's modulus, *Poisson*'s ratio and shear modulus, respectively, as

$$[S] = \begin{bmatrix} 1/E_L & -\nu_{RL}/E_R & -\nu_{TL}/E_T & 0 & 0 & 0 \\ -\nu_{LR}/E_L & 1/E_R & -\nu_{TR}/E_T & 0 & 0 & 0 \\ -\nu_{LT}/E_L & -\nu_{RT}/E_R & 1/E_T & 0 & 0 & 0 \\ 0 & 0 & 0 & 1/G_{RT} & 0 & 0 \\ 0 & 0 & 0 & 0 & 1/G_{LT} & 0 \\ 0 & 0 & 0 & 0 & 0 & 1/G_{LR} \end{bmatrix}. \qquad (2)$$

Since the compliance matrix is symmetric ($S_{ij} = S_{ji}$), the following relationship must be verified $\nu_{ij}/E_i = \nu_{ji}/E_j$ (i, j = 1,2,3).

Let us consider now the general case in which the material coordinate system is rotated with regard all axes of the specimen coordinate system. In this case,

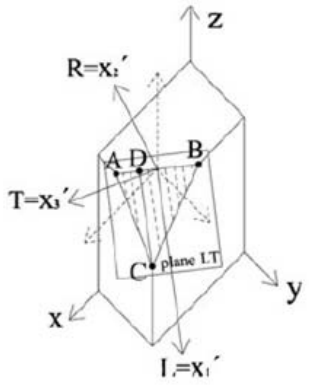

Figure 1: Schematic representation of the off-axis compression test.

the stress state in the material coordinate system ($[\sigma]$) can be determined from the applied stress state in the specimen coordinate system ($[\sigma']$) by the following transformation rule of second-order symmetric tensors

$$[\sigma] = [T]^T [\sigma'] [T], \tag{3a}$$

with

$$[\sigma] = \begin{bmatrix} \sigma_{11} & \sigma_{12} & \sigma_{13} \\ \sigma_{12} & \sigma_{22} & \sigma_{23} \\ \sigma_{13} & \sigma_{23} & \sigma_{33} \end{bmatrix}, \; [\sigma'] = \begin{bmatrix} \sigma_{xx} & \sigma_{xy} & \sigma_{xz} \\ \sigma_{xy} & \sigma_{yy} & \sigma_{yz} \\ \sigma_{xz} & \sigma_{yz} & \sigma_{zz} \end{bmatrix} \text{ and } [T] = \begin{bmatrix} l_1 & l_2 & l_3 \\ m_1 & m_2 & m_3 \\ n_1 & n_2 & n_3 \end{bmatrix} \tag{3b}$$

where $\sigma_{ij} = \tau_{ij}$ when $i \neq j$, $[T]^T$ is the transpose of matrix $[T]$ and l_k, m_k e n_k $(k = 1, 2, 3)$ are the direction cosine between material and specimen coordinate systems. In Voigt notation, Eq. (3) writes

$$\begin{Bmatrix} \sigma_{11} \\ \sigma_{22} \\ \sigma_{23} \\ \tau_{23} \\ \tau_{13} \\ \tau_{12} \end{Bmatrix} = \begin{bmatrix} l_1^2 & m_1^2 & n_1^2 & 2l_1m_1 & 2m_1n_1 & 2l_1n_1 \\ l_2^2 & m_2^2 & n_2^2 & 2l_2m_2 & 2m_2n_2 & 2l_2n_2 \\ l_3^2 & m_3^2 & n_3^2 & 2l_3m_3 & 2m_3n_3 & 2l_3n_3 \\ l_1l_2 & m_1m_2 & n_1n_2 & l_1m_2 + l_2m_1 & m_1n_2 + m_2n_1 & l_1n_2 + l_2n_1 \\ l_2l_3 & m_2m_3 & n_2n_3 & l_2m_3 + l_3m_2 & m_2n_3 + m_3n_2 & l_2n_3 + l_3n_2 \\ l_1l_3 & m_1m_3 & n_1n_3 & l_1m_3 + l_3m_1 & m_1n_3 + m_3n_1 & l_1n_3 + l_3n_1 \end{bmatrix} \begin{Bmatrix} \sigma_{xx} \\ \sigma_{yy} \\ \sigma_{zz} \\ \tau_{yz} \\ \tau_{xz} \\ \tau_{xy} \end{Bmatrix} \tag{4a}$$

or

$$\{\sigma\} = [T_{\sigma'\sigma}] \{\sigma'\}. \tag{4b}$$

In the same way, the strain tensor in the material and specimen coordinate system are transformed by the following rule

$$[\varepsilon] = [T]^T [\varepsilon'][T], \tag{5a}$$

with

$$[\varepsilon] = \begin{bmatrix} \varepsilon_{11} & \varepsilon_{12} & \varepsilon_{13} \\ \varepsilon_{12} & \varepsilon_{22} & \varepsilon_{23} \\ \varepsilon_{13} & \varepsilon_{23} & \varepsilon_{33} \end{bmatrix} \text{ and } [\varepsilon'] = \begin{bmatrix} \varepsilon_{xx} & \varepsilon_{xy} & \varepsilon_{xz} \\ \varepsilon_{xy} & \varepsilon_{yy} & \varepsilon_{yz} \\ \varepsilon_{xz} & \varepsilon_{yz} & \varepsilon_{zz} \end{bmatrix} \tag{5b}$$

where $\varepsilon_{ij} = \gamma_{ij}/2$ when $i \neq j$. In Voigt notation, Eq. (5) writes

$$\begin{Bmatrix} \varepsilon_{11} \\ \varepsilon_{22} \\ \varepsilon_{23} \\ \gamma_{23} \\ \gamma_{13} \\ \gamma_{12} \end{Bmatrix} = \begin{bmatrix} l_1^2 & m_1^2 & n_1^2 & l_1 m_1 & m_1 n_1 & l_1 n_1 \\ l_2^2 & m_2^2 & n_2^2 & l_2 m_2 & m_2 n_2 & l_2 n_2 \\ l_3^2 & m_3^2 & n_3^2 & l_3 m_3 & m_3 n_3 & l_3 n_3 \\ 2l_1 l_2 & 2m_1 m_2 & 2n_1 n_2 & l_1 m_2 + l_2 m_1 & m_1 n_2 + m_2 n_1 & l_1 n_2 + l_2 n_1 \\ 2l_2 l_3 & 2m_2 m_3 & 2n_2 n_3 & l_2 m_3 + l_3 m_2 & m_2 n_3 + m_3 n_2 & l_2 n_3 + l_3 n_2 \\ 2l_1 l_3 & 2m_1 m_3 & 2n_1 n_3 & l_1 m_3 + l_3 m_1 & m_1 n_3 + m_3 n_1 & l_1 n_3 + l_3 n_1 \end{bmatrix} \begin{Bmatrix} \varepsilon_{xx} \\ \varepsilon_{yy} \\ \varepsilon_{zz} \\ \gamma_{yz} \\ \gamma_{xz} \\ \gamma_{xy} \end{Bmatrix} \tag{6a}$$

or

$$\{\varepsilon\} = [T_{\varepsilon'\varepsilon}] \{\varepsilon'\}. \tag{6b}$$

The transformation matrices of stress ($[T_{\sigma'\sigma}]$) and strain ($[T_{\varepsilon'\varepsilon}]$) satisfy the following properties

$$[T_{\sigma'\sigma}]^{-1} = [T_{\varepsilon'\varepsilon}]^T \quad \text{and} \quad [T_{\varepsilon'\varepsilon}]^{-1} = [T_{\sigma'\sigma}]^T. \tag{7}$$

The transformation of the compliance matrix $[S]$, between material and specimen coordinate systems, can be deduced from the above Eqs (3-7). Starting from Eq. (1) one gets

$$\{\varepsilon\} = [S]\{\sigma\} \Leftrightarrow [T_{\varepsilon'\varepsilon}]\{\varepsilon'\} = [S][T_{\sigma'\sigma}]\{\sigma'\} \Leftrightarrow \{\varepsilon'\} = [T_{\sigma'\sigma}]^T [S][T_{\sigma'\sigma}]\{\sigma'\}. \tag{8}$$

Therefore, in an arbitrary off-axes configuration, the Hooke's law in the specimen coordinate system is given by

$$\begin{Bmatrix} \varepsilon_{xx} \\ \varepsilon_{yy} \\ \varepsilon_{zz} \\ \gamma_{yz} \\ \gamma_{xz} \\ \gamma_{xy} \end{Bmatrix} = \begin{bmatrix} S'_{11} & S'_{12} & S'_{13} & S'_{14} & S'_{15} & S'_{16} \\ S'_{12} & S'_{22} & S'_{23} & S'_{24} & S'_{25} & S'_{26} \\ S'_{13} & S'_{23} & S'_{33} & S'_{34} & S'_{35} & S'_{36} \\ S'_{14} & S'_{24} & S'_{34} & S'_{44} & S'_{45} & S'_{46} \\ S'_{15} & S'_{25} & S'_{35} & S'_{45} & S'_{55} & S'_{56} \\ S'_{16} & S'_{26} & S'_{36} & S'_{46} & S'_{56} & S'_{66} \end{bmatrix} \begin{Bmatrix} \sigma_{xx} \\ \sigma_{yy} \\ \sigma_{zz} \\ \tau_{yz} \\ \tau_{xz} \\ \tau_{xy} \end{Bmatrix} \quad \Rightarrow \quad \{\varepsilon\} = [S]\{\sigma\} \tag{9}$$

with,

$$[S'] = [T_{\sigma'\sigma}]^T [S][T_{\sigma'\sigma}]. \tag{10}$$

From the anisotropic elasticity theory, it is possible to derive an explicit relationship linking unknown compliance coefficients with specimen dimensions, loading configuration and strain measurements as

$$[T_{\varepsilon'\varepsilon}] \{\varepsilon'\} = [S][T_{\sigma'\sigma}] \{\sigma'\} \tag{11}$$

in which,

- $[T_{\varepsilon'\varepsilon}]$ and $[T_{\sigma'\sigma}]$: are transformation matrices whose elements are cosine directions defined in function of the off-axis angles between material and specimen coordinates systems;
- $\{\varepsilon'\}$: lists the strain components across the gauge section in the specimen coordinate system;
- $\{\sigma'\}$: lists the stress state applied to the specimen (applied load).
- $[S]$: is a function of the components of the compliance matrix completely defining the orthotropic behaviour of the material.

In practice, the strain components at the gauge section ($\{\varepsilon'\}$) can be determined by a suitable full-field optical method, as for instance, 3D digital image correlation. When the orthotropic material can be assumed homogeneous, an average value over the gauge section can be determined.

Given an off-axes configuration, let us consider a first loading case consisting in a uniaxial compression stress along the x direction

$$\{\sigma_x\} = \left\{F/A, \quad 0, \quad 0, \quad 0, \quad 0, \quad 0\right\}^T. \tag{12}$$

In this case the linear system of Eqs. (11) can be re-written as

$$\sigma_{xx} \begin{bmatrix} l_1^2 & l_2^2 & l_3^2 & 0 & 0 & 0 & 0 & 0 & 0 \\ 0 & l_1^2 & 0 & l_2^2 & l_3^2 & 0 & 0 & 0 & 0 \\ 0 & 0 & l_1^2 & 0 & l_2^2 & l_3^2 & 0 & 0 & 0 \\ 0 & 0 & 0 & 0 & 0 & 0 & l_1 l_2 & 0 & 0 \\ 0 & 0 & 0 & 0 & 0 & 0 & 0 & l_2 l_3 & 0 \\ 0 & 0 & 0 & 0 & 0 & 0 & 0 & 0 & l_1 l_3 \end{bmatrix} \begin{Bmatrix} S_{11} \\ S_{12} \\ S_{13} \\ S_{22} \\ S_{23} \\ S_{33} \\ S_{44} \\ S_{55} \\ S_{66} \end{Bmatrix} = [T_{\varepsilon'\varepsilon}] \{\varepsilon'\} \tag{13a}$$

or, in compact form

$$[A_x]\{S\} = \{b_x\} \tag{13b}$$

The system of Eqs. (13) is undetermined since there are only six equations for nine unknowns compliance elements. In order to solve this linear system, a possibility is considering at least two independent loading cases. In practice, this can be achieved by carrying out the compression test along different loading axis, as for instance,

- Uniaxial loading case 1:
  $\{\sigma_x\} = \{F/A, 0, 0, 0, 0, 0\}^T \implies [A_x]\{S\} = \{b_x\}$
- Uniaxial loading case 2:
  $\{\sigma_y\} = \{0, F/A, 0, 0, 0, 0\}^T \implies [A_y]\{S\} = \{b_y\}$
- Uniaxial loading case 3:
  $\{\sigma_z\} = \{0, 0, F/A, 0, 0, 0\}^T \implies [A_z]\{S\} = \{b_z\}$

This approach yields to an overdetermined system of equation which can be solved with regard to the compliance components ($\{S\}$) using the concept of pseudo-inverse. Generically, for the three compression loading systems, Eqs. (13) can be re-write as

$$\begin{bmatrix}[A_x]\\ [A_y]\\ [A_z]\end{bmatrix}\{S\} = \begin{bmatrix}\{b_x\}\\ \{b_y\}\\ \{b_z\}\end{bmatrix} \tag{14a}$$

or, in compact form

$$[R]\{S\} = \{q\}\,. \tag{14b}$$

Finally, Eqs. (14) can then be solved as

$$\{S\} = ([R]^{-1}[R])^{-1}[R]^{-1}\{q\}\,. \tag{15}$$

3. Finite element analyses

3.1. Finite element model

A 3D finite element model of the off-axis compression test was built in ANSYS® 14. Clear wood was modelled as a continuous and homogeneous medium with an orthotropic linear elastic behaviour. Maritime pine (*Pinus pinaster* Ait.) was considered with properties as summarised in Table 1 [2]. According to the experimental work, the dimensions of the specimen were taken equal to 68(R)×36(T)×33(L) mm [1]. The 3D 8-node structural SOLID185 was selected from the element library.

Table 1: Engineering constants of maritime pine used in finite element analyses [2].

E_L (GPa)	E_R (GPa)	E_T (GPa)	ν_{RT} (-)	ν_{TL} (-)	ν_{LR} (-)	G_{RT} (GPa)	G_{LT} (GPa)	G_{LR} (GPa)
15.1	1.91	1.01	0.59	0.051	0.47	0.286	1.22	1.41

The ANEL anisotropic elastic model was used for material parameter definition. A mesh with 37407 nodes and 34370 elements was defined (Fig. 2). The element size was set to 1.25 mm, which is an order of magnitude higher than the displacement spatial resolution that can be typically achieved experimentally by a digital image correlation technique. No symmetry of the model about the y and z axes was taken into account, so the numerically deformation across the whole lateral surfaces could be processed exactly as performed experimentally [1].

The compression test was simulated by contact boundary conditions. The compression plates were simulated by a rigid surface TARGE170 element. CONTA173 element was selected for simulating the contact interface between bottom and top surfaces of the model and the target rigid surface. Degree of freedom (translations and rotations) were then applied to target nodes simulating the compression test in the linear elastic domain. The friction coefficient of 0.5 was firstly chosen, but it can be changed according to the experimental procedure for reduction of friction effects.

The convergence of the model (mesh and contact boundary conditions) was checked assuming a compression test parallel to the grain (*i.e.*, in which material and specimen coordinate systems were coincident) based on a specimen with nominal dimensions of 25(R)×25(T)×100(L) mm according to the ASTM D 143 standard [3] (longitudinal direction L parallel to the y axis of the specimen). From the numerical deformation at an external surface, a longitudinal modulus of elasticity was determined according to the following closed-form solution (data reduction): $E_L = (P/A)/\varepsilon_L$, where P represents the global applied load, A is the cross-section of the specimen and ε_L is the axial strain along the longitudinal direction. Numerically, P was determined as the vertical reaction force at the upper target nodes. Moreover, ε_L was defined as the average value of the nodal y axial strains within a central area of 5×5 mm (this area could correspond experimentally to the measuring region covered by a strain gauge or an optical method). The error between the calculated and reference E_L values was negligible.

3.2. Identifiability analyses

The finite element model presented before will be used in further analyses in order to investigate boundary effects on the mechanical response of the specimen. Moreover, it will be used to optimise the test configuration in terms of grain

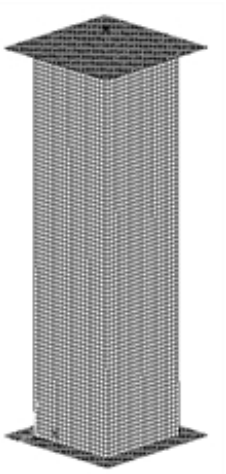

Figure 2: Finite element model of the off-axis compression test.

orientation with regard to the identifiability of all active stiffness components. The angles orientation (rotation transformation matrix) can be defined by following three basic rotation matrices corresponding to elementary rotations about the x, y, and z axis

$$[R_x(\theta_L)] = \begin{bmatrix} 1 & 0 & 0 \\ 0 & \cos\theta_L & \sin\theta_L \\ 0 & -\sin\theta_L & \cos\theta_L \end{bmatrix} \tag{16a}$$

$$[R_y(\theta_R)] = \begin{bmatrix} \cos\theta_R & 0 & -\sin\theta_R \\ 0 & 1 & 0 \\ \sin\theta_R & 0 & \cos\theta_R \end{bmatrix} \tag{16b}$$

$$[R_z(\theta_T)] = \begin{bmatrix} \cos\theta_T & \sin\theta_T & 0 \\ -\sin\theta_T & \cos\theta_T & 0 \\ 0 & 0 & 1 \end{bmatrix} \tag{16c}$$

in which, the final rotation transformation matrix will then be given by

$$\begin{aligned} [R_t] &= [R_z(\theta_T)][R_y(\theta_R)][R_x(\theta_L)] \\ &= \begin{bmatrix} l_1 & l_2 & l_3 \\ m_1 & m_2 & m_3 \\ n_1 & n_2 & n_3 \end{bmatrix} \end{aligned} \tag{16d}$$

where (L_i, m_i, n_i) are the direction cosines of $\mathbf{e}_i$ $(i = 1, 2, 3)$ with regard to the

global coordinate system $S(0, \mathbf{i}, \mathbf{j}, \mathbf{k})$. For the purpose of optimum test configuration, a cost function can be defined as

$$\phi(\theta_L, \theta_R, \theta_T) = \frac{\triangle}{6(\varepsilon_1^2 + \varepsilon_2^2 + \varepsilon_3^2 + \gamma_{23}^2 + \gamma_{13}^2 + \gamma_{12}^2)}. \tag{17a}$$

with

$$\begin{aligned} \triangle \;=\; & (\varepsilon_1 - \varepsilon_2)^2 + (\varepsilon_1 - \varepsilon_3)^2 + (\varepsilon_1 - \gamma_{23})^2 + (\varepsilon_1 - \gamma_{13})^2 + (\varepsilon_1 - \gamma_{12})^2 \\ & + (\varepsilon_2 - \varepsilon_3)^2 + (\varepsilon_2 - \gamma_{23})^2 + (\varepsilon_2 - \gamma_{13})^2 + (\varepsilon_2 - \gamma_{12})^2 \\ & + (\varepsilon_3 - \gamma_{23})^2 + (\varepsilon_3 - \gamma_{13})^2 + (\varepsilon_3 - \gamma_{12})^2 \\ & + (\gamma_{23} - \gamma_{13})^2 + (\gamma_{23} - \gamma_{12})^2 + (\gamma_{13} - \gamma_{12})^2 \end{aligned} \tag{17b}$$

Eventually, the minimisation of the cost function, $\phi(\theta_i)$ $(i = L, R, T)$ (Eq. 17), should yield a configuration in which the strain components are balanced out and evenly spread across the gauge section. Therefore, this configuration should correspond to an optimum configuration for the multi-parameter identification purposes.

The strain components on the material coordinate system figuring in the cost function of Eq. (17) can be deduced analytically from the anisotropic elasticity theory. From this theory and assuming a uniaxial stress state along the x axis $(\sigma_x = \varepsilon_x / S'_{11})$ the following expression can be obtained

$$\begin{aligned} \varepsilon_1/\varepsilon_x &= (S_{11} l_1^2 + S_{12} l_2^2 + S_{13} l_3^2)/S'_{11} \\ \varepsilon_2/\varepsilon_x &= (S_{12} l_1^2 + S_{22} l_2^2 + S_{23} l_3^2)/S'_{11} \\ \varepsilon_3/\varepsilon_x &= (S_{13} l_1^2 + S_{23} l_2^2 + S_{33} l_3^2)/S'_{11} \\ \gamma_{23}/\varepsilon_x &= (S_{44} l_1 l_2)/S'_{11} \\ \gamma_{13}/\varepsilon_x &= (S_{55} l_2 l_3)/S'_{11} \\ \gamma_{12}/\varepsilon_x &= (S_{66} l_1 l_3)/S'_{11} \end{aligned} \tag{18a}$$

with

$$S'_{11} = S_{11} c^4 - 2S_{16} c^3 s + (2S_{12} + S_{66}) c^2 s^2 - 2S_{26} c s^3 + S_{22} s^4 \tag{18b}$$

Assuming reference properties of a given wood species Eqs. (18) can be used in the minimisation process of optimum off-axes angle orientation (Eq. 17) of the prismatic specimen. Fig. 3 shown the evaluation of Eq. (17) with regard to off-axis angles θ_L $(\theta_R = \theta_T = 0)$, θ_R $(\theta_L = \theta_T = 0)$, θ_T $(\theta_L = \theta_R = 0)$. From this preliminary result, it can be concluded that this cost function is more sensitive to θ_R and θ_T than to θ_L. Moreover, angles of about $\theta_R = 29°$ and $\theta_T = 9°$ should yield better identification stiffness values.

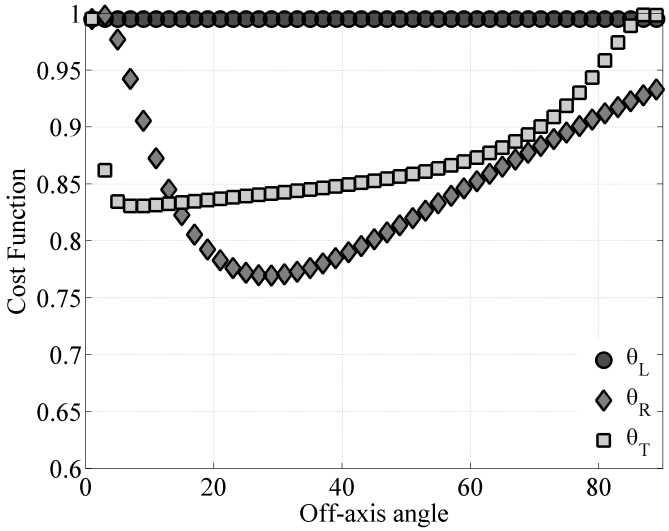

Figure 3: Evaluation of cost function (Eq. 17) with regard to off-axis angle θ_L ($\theta_R = \theta_T = 0$), θ_R ($\theta_L = \theta_T = 0$), θ_T ($\theta_L = \theta_R = 0$).

4. Experimental work

4.1. Material and specimens

The material used in this work was wood with nominal dimensions of 60×40×40 mm and arbitrary orientation between material and coordinate systems. The rotation angles (Eq. 16) were determined after testing according to the procedure described in [1]. Before testing, the specimens were conditioned at a room temperature of 20±2°C and 65±5%.

4.2. Stereovision measurements

The stereovision or 3D digital image correlation method (3D-DIC) was chosen in this work. This is a white-light optical technique which provides the 3D displacement field over plane or moderate curved surfaces [4, 5]. It can be more easily coupled with conventional apparatus such as a universal testing machine than an interferometric counterpart (namely because no specific equipment such as a laser or an anti-vibration table is required). Besides, considering the biological nature of the material, this technique has the advantage of being non-intrusive and requires simpler specimen preparation (speckle pattern) then other white-light techniques such as grid methods [6, 7]. Moreover, the utilisation of a stereovision system was advantageous in practice because: (i) a pair of lateral surfaces on the compression test could be measured simultaneously; (ii) a measurement volume is defined through the calibration procedure of the stereovision system, therefore specimens can be flexibility positioned and aligned as long as they fit into this

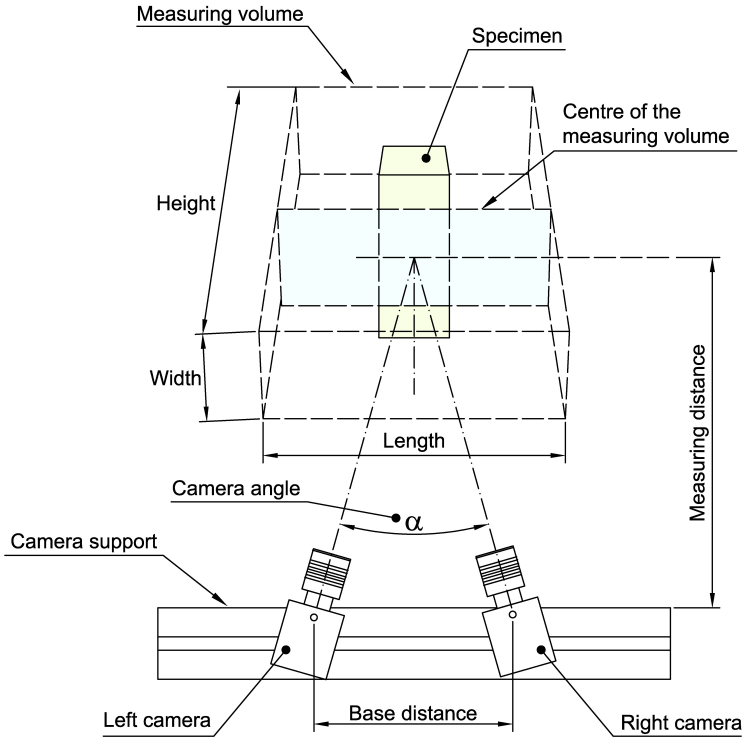

Figure 4: Finite element model of the off-axis compression test.

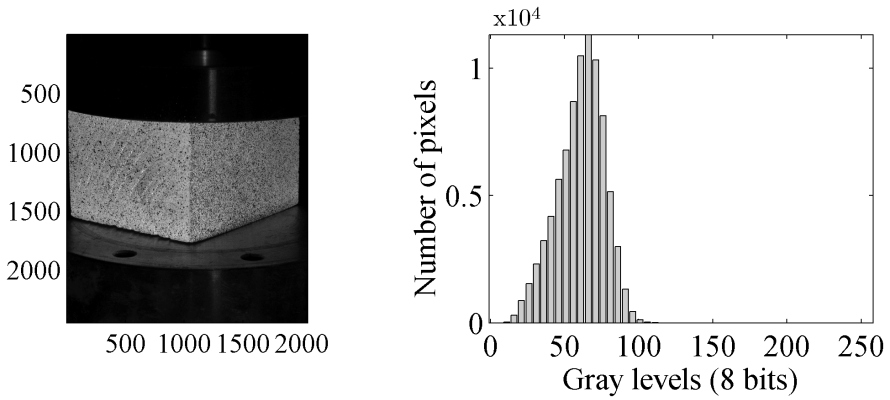

Figure 5: Finite element model of the off-axis compression test.

virtual space. However, when compared to a monovision system (DIC-2D), the main disadvantage is that the uncertainty on the evaluation of the parameters of the camera model represents an additional uncertainty on the displacement measurement, and therefore on the evaluation of the material parameters.

The stereovision technique is a full-field technique for measuring the 3D (in-plane and out-of-plane) displacement/strain fields of a given 3D object. The analysis is based on a sequence of pair of stereo images recorded during the object deformation. A binocular stereovision (a measuring system with a pair of left and right cameras) is used for assessing the position of a 3D point in space (with regard to a given world coordinate system) from the knowledge of its stereo projection points in the two recorded images (Fig. 4). This process is known as triangulation. On the one hand, this method requires a camera calibration consisting in determining the extrinsic (the relative position and orientation of the coordinates systems associated to the two cameras) and intrinsic parameters of the camera model. On the other hand, a correspondence of the projection points on the two cameras must be established (stereo-matching problem) using for instance the epipolar constant concept.

The digital image correlation method is based on the assumption that the surface of the object under analysis has a textured pattern such that the light intensity, diffusely reflected over the surface, will vary continuously with a suitable contrast. Different techniques have been successfully used for the creation of such a speckle pattern, employing spray or airbrush paint, toner powder deposit or lithography. In this work, the speckle pattern was created by aerosol spray, applying a thin coating of white paint followed by a spot distribution of black paint (Fig. 5).

In the DIC method, the displacement field is measured by analysing the geometrical deformation of the images of the surface of interest, recorded before and

Table 2: Measuring parameters.

Project parameter – Facet	
Facet size	15×15 pixels
Step size	13×13 pixels
Project parameter – Strain	
Computation size	5×5 facets
Validity code	55%
Strain computation method	Total
Image recording	
Acquisition frequency	1 Hz

after deformation. For this purpose, the initial (undeformed) image is mapped by correlation windows (facets), within which an independent measurement of the displacement is calculated. Therefore, the facet size on the object plane will define the spatial resolution of the displacement. Typically, a great facet size will improve the precision of the measurements but also will degrade the spatial resolution. Thus, a compromise must be found according to the application to be handled. In this work, a facet size of 15×15 pixels was chosen, attending to the size of the region of interest, the optical system (magnification) and the quality of the granulate (average speckle size) obtained by the spray painting (Table 1). The facet step was set to 13×13 pixels allowing an overlapping of 2 pixels (Table 1), in order to enhance spatial resolution. The in-plane displacements were then numerically differentiated in order to determine the strain field needed for the material characterisation problem on a base computation size of 5 subsets (Table 1).

To estimate the accuracy of the measuring system, motionless tests were performed after calibration, consisting in recording several images of a target object without applying any deformation. These images were then processed based on the digital image correlation, in order to compute the 3D full-field displacements. Noisy maps were typically obtained following a Gaussian normal distribution as shown in Fig. 6. The resolution in both displacement and strain associated to the 3D full-fiel measurements were estimated as the standard deviation of these noise fields. The resolution of in-plane displacements (u_x, u_y) were in the range of 0.54 μm, whilst a value of about 2.40 μm was reached for the out-of-plane displacement (u_z) (field of view of 36.1 × 64.7 mm). The strain resolution was estimated about 0.011 %. Besides, as it can be concluded from the normal distribution (Fig. 6), no significant systematic (bias) errors occur.

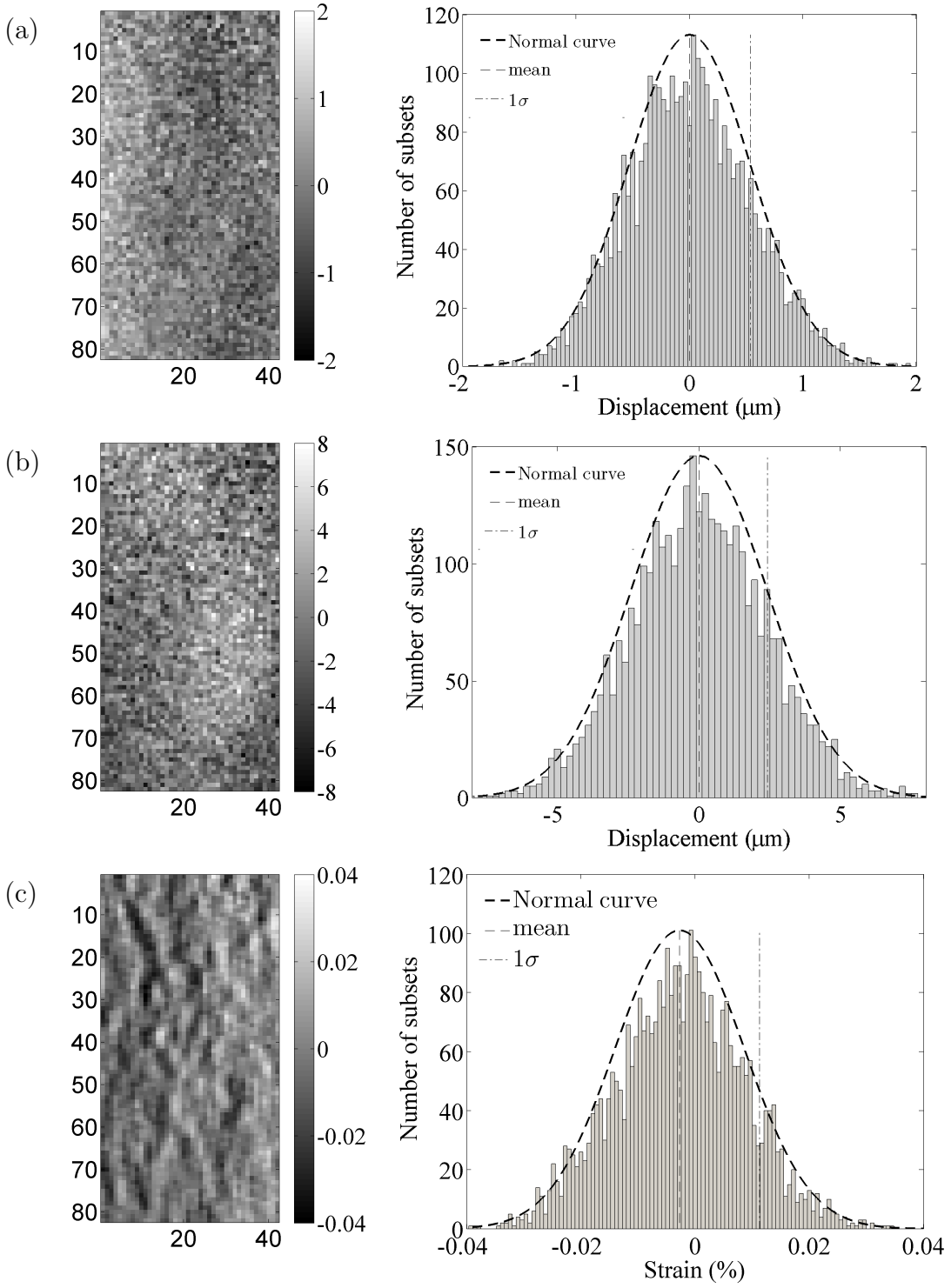

Figure 6: Estimation of the resolution associated to DIC-3D (a) X displacement component (σ_{u_x} = 0.54 μm); (b) Z displacement component (σ_{u_z} = 2.40 μm); (c) X strain component (σ_{ε_x} = 0.011 %) (Field of view : 36.1 × 64.7 mm).

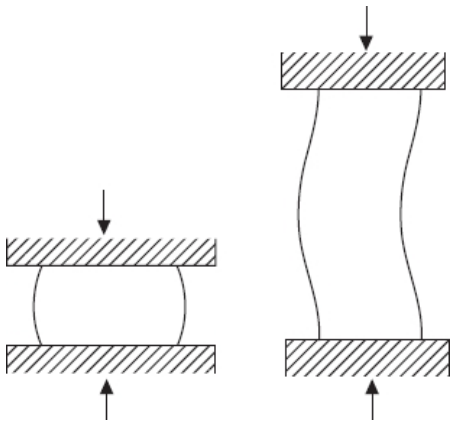

Figure 7: Problems with compression test: (right) Friction at the ends prevents spreading, which results in barreling; (left) buckling effects.

4.3. Compression test

A compression test on a rectangular prismatic specimen was proposed in this work. In order to be meaningful, friction and buckling effects must be avoid or minimised when carrying out a compression test. Friction between specimen and platens tend to prevent the lateral spreading of material near the ends, eventually inducing a barrel-like shape deformation of the specimen (Fig. 7). Friction can be reduced by using a lubricant promoting the free movement of the specimen at the contact surface. Friction can also be reduced by increasing the height-to-width/thickness ratio, but this ratio must be chosen in order to prevent buckling. Tests were carry out on a servo-hydraulic tensile machine under displacement control with a rate of 0.2 mm/min. The load cell was measured by means of a load cell of 100 kN capacity.

5. Preliminary results, conclusions and future work

A first set of results are summarised in Fig. 8 [1]. By comparing these results with literature values reported in Table 3, one can conclude that reasonable agreement can be found among the engineering constants. Although improvements should be achieved in the identifiability of some elastic properties as for instance the Young's modulus along the grain (E_L).

In future collaborations the following issued are to be addressed:

- Optimisation of the off-axes compression test method with regard to boundary conditions and off-axes angle orientation (balancing out strain components on the material coordinate system);

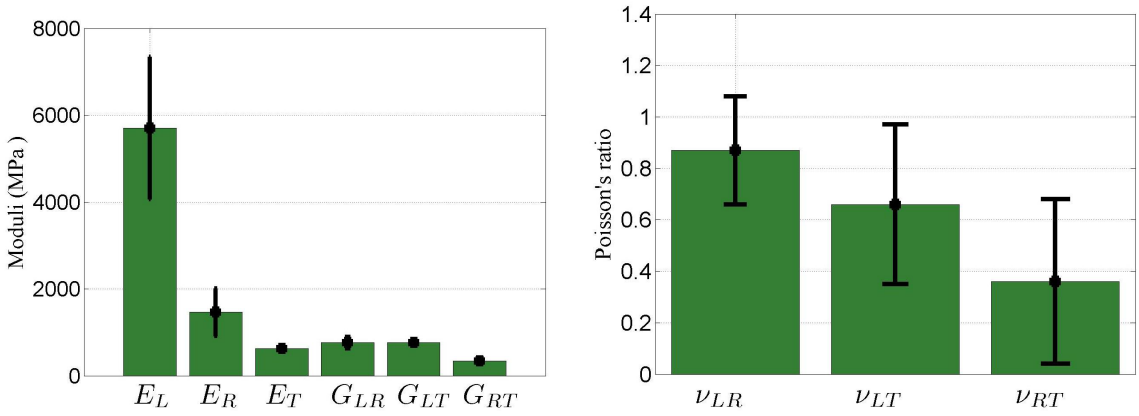

Figure 8: Engineering constants measured from the proposed off-axes compression test [1].

Table 3: Literature reference properties of softwood species.

E_L (MPa)	E_R (MPa)	E_T (MPa)	G_{LR} (MPa)	G_{LT} (MPa)	G_{RT} (MPa)	ν_{LR}	ν_{LT}	ν_{RT}
11400-16103	1500	800-1353	900	600-1228	255-280	0.3-0.46	0.3-0.52	0.68-0.71

- Utilization of interferometric optical method for enhance resolution associated to the strain tensor;

So far, in the result of this STSM the following publications are envisaged:

[1] Xavier, J.; Majano-Majano, A.; Fernandez-Cabo, J. Identifiability of stiffness components of clear wood from a single off-axes compression test. 15th International Conference on Experimental Mechanics, Faculty of Engineering, University of Porto, Portugal, 22-27 July, 2012;

[2] Majano-Majano, A.; Fernandez-Cabo, J.; Xavier, J. Characterization of clear wood by a single specimen: evaluation of first results and further improvements. 6th European Congress on Computational Methods in Applied Sciences and Engineering (ECCOMAS 2012), Vienna, Austria, 10-14 September, 2012;

Acknowledgments

The authors gratefully acknowledge the COST Action FP1004 "Enhance mechanical properties of timber, engineered wood products and timber structures" for the financial support of the Short Term Scientific Mission: COST-STSM-FP1004-10687.

References

[1] A. Majano-Majano, J. Fernandez-Cabo, S. Hoheisel, M. Klein, A test method for characterizing clear wood using a single specimen, Experimental Mechanics 1 (1) (2012) 1–18.

[2] J. Xavier, N. Garrido, J. Oliveira, J. Morais, P. Camanho, F. Pierron, A comparison between the Iosipescu and off-axis shear test methods for the characterization of *pinus pinaster* Ait., Composites Part A: Applied Science and Manufacturing 35 (7-8) (2004) 827–840.

[3] ASTM D143, Standard methods of testing small clear specimens of timber, ASTM International, West Conshohocken, PA, 2007.

[4] J.-J. Orteu, 3-D computer vision in experimental mechanics, Optics and Lasers in Engineering 47 (3-4) (2009) 282–291.

[5] M. Sutton, J.-J. Orteu, H. Schreier, Image correlation for shape, motion and deformation measurements: Basic concepts, theory and applications, Springer, 2009.

[6] J. Xavier, S. Avril, F. Pierron, J. Morais, Novel experimental approach for longitudinal-radial stiffness characterisation of clear wood by a single test, Holzforschung 61 (5) (2007) 573–581.

[7] J. Xavier, S. Avril, F. Pierron, J. Morais, Variation of transverse and shear stiffness properties of wood in a tree, Composites Part A: Applied Science and Manufacturing 40 (2009) 1953–1960.